

Integrated Sensing, Communication, and Computation Over-the-Air in OFDM Systems

Biao Dong, Bin Cao, *Member, IEEE*, and Qinyu Zhang, *Senior Member, IEEE*

Abstract—This work is concerned with integrated sensing, communication, and computation (ISCC) in uplink orthogonal frequency division multiplexing (OFDM) systems, wherein multiple devices perform target sensing and over-the-air computation (AirComp) simultaneously. We aim to minimize the computational mean squared error (MSE) by jointly optimizing the transmitting vector and the aggregation vector. To tackle the non-convexity of this problem, we develop a two-phase iterative algorithm. Simulations demonstrate the effectiveness of the proposed algorithm.

Index Terms—Integrated sensing and communication, over-the-air computation, OFDM, integrated sensing, communication, and computation.

I. INTRODUCTION

Next-generation wireless sensor networks (WSNs) have been envisioned to be a multi-functional network, which can support various communication-intensive, latency-sensitive, and computation-heavy applications. Towards this end, integrated sensing and communications (ISAC) is regarded as a key technology, which can share the same resources, hardware infrastructure, and signal processing modules within a single platform [1].

The existing ISAC research mainly focuses on the deep integration of sensing and communication at a single base station. In practical scenarios, numerous ISAC devices interconnect to form a network that simultaneously collects and transmits data while performing real-time computation at one access point (AP), as shown in Fig. 1. How to integrate computing functionality into existing ISAC network and further form integrated sensing, communication, and computation (ISCC) system has attracted extensive attention (see [2] and the references therein).

Recently, over-the-air computation (AirComp) has been introduced into ISAC systems for ultrafast data aggregation and computation [3]–[6]. As a promising multiple access technology, AirComp exploits the signal-superposition property of a multi-access channel to compute a class of so-called nomographic functions of distributed sensing data via concurrent device transmissions. In [3], a unified integrated sensing and communication (ISCC) framework was proposed, which focuses on integrating sensing and AirComp while minimizing computational error under communication threshold constraints. [4] further considered the delivery of sensed data, wherein antenna arrays at each device support radar sensing

and AirComp. [5] analyzed the impacts of antenna array structures and beampatterns. [6] focused on jointly optimizing ISCC with downstream tasks in a task-oriented manner to achieve low-latency edge inference.

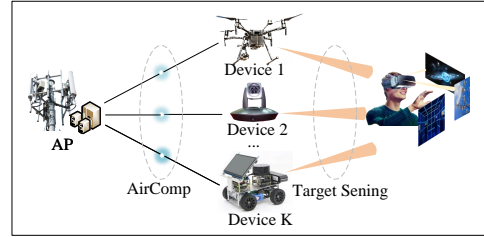


Fig. 1. The considered ISCC system comprises one common target and one AP. Each radar device simultaneously transmit probing signals to detect the target and data symbols to the AP for AirComp. Each radar is equipped with a single antenna for signal transmitting and sensing, while the AP is also equipped with a single antenna for signal aggregation.

In this letter, we extend the ISCC to orthogonal frequency division multiplexing (OFDM) systems operating over frequency-selective fading channels. Unlike previous works based on single-carrier transmission [3]–[6], we aim to minimize the computational mean squared error (MSE) on all sub-carriers via joint optimization of transceiver vectors, subject to Cramér-Rao lower bound (CRLB) and power constraints. To tackle this non-convex problem, we propose a two-phase iterative optimization algorithm, consisting of a successive convex approximation (SCA)-based alternating optimization (AO) phase and an alternating direction method of multipliers (ADMM)-based refinement phase. These two phases respectively focus on decoupling and relaxation of non-convex problems, as well as exploring a broader feasible region. Numerical results show that the proposed method achieves a better computing-sensing trade-off compared with the baseline.

II. SYSTEM MODEL AND PROBLEM FORMULATION

A. System Model

1) *AirComp Model*: We denote the index of symbol durations by $m \in \mathcal{M} = \{1, \dots, M\}$ and consider the m -th OFDM signal for AirComp

$$\mathbf{C}_k = [C_{k,0}, \dots, C_{k,N-1}]^T \in \mathbb{C}^{N \times 1} \quad (1)$$

which denotes normalized measured data vector from device $k \in \mathcal{K} = \{1, \dots, K\}$ on N subcarriers¹. Here, \mathbf{C}_k is assumed to be independent and identically distributed (i.i.d.) among different devices, i.e., $\mathbb{E}[C_{i,n} C_{i,n}^*] = 1$, $\mathbb{E}[C_{i,n} C_{j,n}^*] = 0$, $\forall n \in$

¹To simplify the notation, we ignore the subscript m of each subcarrier element \mathbf{C}_k^m in \mathbf{C}_k .

Biao Dong, Bin Cao, and Qinyu Zhang are with the School of Electronic and Information Engineering, Harbin Institute of Technology (Shenzhen), Shenzhen 518055, China (e-mail: 23b952012@stu.hit.edu.cn; caobin@hit.edu.cn; zqy@hit.edu.cn).

$\mathcal{N}, i, j \in \mathcal{K}, i \neq j$. AirComp aims to calculate the average value of all devices on a certain subcarrier as

$$F_n = \frac{1}{K} \sum_{k=1}^K C_{k,n}, \quad \forall n \in \mathcal{N}. \quad (2)$$

In addition, $\mathbf{X}_k = [X_{k,0}, \dots, X_{k,N-1}]^T \in \mathbb{C}^{N \times 1}$ is the transmitted signal given by $\mathbf{X}_k = \mathbf{B}_k \circ \mathbf{C}_k$, where $\mathbf{B}_k = [B_{k,0}, \dots, B_{k,N-1}]^T \in \mathbb{C}^{N \times 1}$ is the frequency domain transmitting vector. Each device satisfies the power constraint as follows

$$\sum_{n=0}^{N-1} \mathbb{E}[|X_{k,n}|^2] = \|\mathbf{B}_k\|^2 \leq P_t, \forall k \in \mathcal{K}, m \in \mathcal{M}. \quad (3)$$

Accordingly, the time domain OFDM signal at sample s generated by device k after the inverse discrete Fourier transform (IDFT) is

$$x_{k,s} = \frac{1}{\sqrt{N}} \sum_{n=0}^{N-1} X_{k,n} e^{j \frac{2\pi}{N} sn} \quad \forall k \in \mathcal{K}, s \in \mathcal{N}. \quad (4)$$

Next, adding cyclic prefix (CP) with length N_c as

$$\mathbf{x}_k = [x_{k,N-N_c}, \dots, x_{k,N-1}]^T \in \mathbb{C}^{(N+N_c) \times 1}. \quad (5)$$

Assume that the wireless channel from device k to the AP has a memory of length L_{dA} , characterized by the taps $\{h_{k,1}, \dots, h_{k,L_{dA}}\}$. Accordingly, the received signal can be expressed as

$$y_s = \sum_{k=0}^{K-1} \sum_{l=0}^{L_{dA}-1} h_{k,l} x_{k,s-\tau_{k,l}} + \omega_s, \forall s \in \mathcal{N} \quad (6)$$

where $\tau_{k,l}$ denotes the delayed arrival of the l -th path and $\omega_s \sim \mathcal{N}(0, \sigma_\omega^2)$ denotes additive white Gaussian noise (AWGN). Performing the discrete Fourier transform (DFT) on the received signal, we have

$$\mathbf{Y}_n = \sum_{k=0}^{K-1} \mathbf{H}_{k,n} \mathbf{B}_{k,n} \mathbf{X}_{k,n} + \Omega_n, \forall n \in \mathcal{N} \quad (7)$$

where $\Omega_n = \frac{1}{\sqrt{N}} \sum_{n=0}^{N-1} \omega_s e^{-j \frac{2\pi}{N} ns}$ denotes the AWGN with distribution $\mathcal{N}(0, \sigma_\omega^2)$ and $\mathbf{H}_{k,n} = \frac{1}{\sqrt{L}} \sum_{l=0}^{L_{dA}-1} h_{k,l} e^{-j \frac{2\pi}{N} ln}$. Next, the AP performs the post-processing using the aggregation vector $\mathbf{W} = [W_1, \dots, W_N]^T \in \mathbb{C}^{N \times 1}$ as

$$\hat{F}_n = \frac{1}{K} \mathbf{W}_n^H \mathbf{Y}_n, \quad \forall n \in \mathcal{N}. \quad (8)$$

where \hat{F}_n is the average value computed from the signals received at the n -th subcarrier across K devices.

Finally, the MSE between the ground truth F_n and the estimated value \hat{F}_n is computed to quantify the computation performance, which is defined as

$$\begin{aligned} \text{MSE} &= \mathbb{E} \left[\frac{1}{N} \sum_{n=1}^{N-1} |\hat{F}_n - F_n|^2 \right] \\ &= \frac{1}{NK^2} \sum_{n=1}^{N-1} \left(\underbrace{\sum_{k=0}^{K-1} |\mathbf{W}_n^H \mathbf{H}_{k,n} \mathbf{B}_{k,n} - 1|^2}_{\text{Signal misalignment error}} + \underbrace{\|\mathbf{W}_n\|^2 \sigma_\Omega^2}_{\text{Noise-induced error}} \right). \end{aligned} \quad (9)$$

where the first term is the signal misalignment error from the residual channel-gain mismatch and the second term is the noise-induced error from the AP. Removing the constant term in (9), we have $\overline{\text{MSE}} = \sum_{n=1}^{N-1} \left(\sum_{k=0}^{K-1} |\mathbf{W}_n^H \mathbf{H}_{k,n} \mathbf{B}_{k,n} - 1|^2 + \|\mathbf{W}_n\|^2 \sigma_\Omega^2 \right)$.

2) *Radar Sensing Model*: Here, we aim to derive the CRLB for the estimation of Doppler and delay using (5). Firstly, we need to derive the received reflected echoes at each device. The target response channel of device k is with the memory of L_{trc} , i.e., $\{g_{k,1}, \dots, g_{k,L_{\text{trc}}}\}$. Similarly, for device k , the interference channel from j -th device $\{g_{j,1}, \dots, g_{j,L_{ic}}\}$ and the direct device channel from j -th device $\{g_{j,1}, \dots, g_{j,L_{ddc}}\}$ [4]. Hence, the target reflection signal received at the k -th device can be expressed as

$$u_{k,s} = \sum_{l=0}^{L_{\text{trc}}-1} g_{k,l} x_{k,s-\tau_{k,l}} e^{j2\pi T_o f_d e^{j\psi}} + \phi_{k,s} + \bar{z}_{k,s}, \quad (10)$$

where $\tau_{k,l}$ denotes the round-trip delay, T_o denotes OFDM symbol duration, f_d denotes Doppler shift, ψ denotes random phase noise, $\phi_{k,s}$ denotes the interference signal as (11) [4] and $\bar{z}_{k,s} \in \mathbb{C}$ is the AWGN with distribution $\mathcal{N}(0, \sigma_z^2)$, which is statistically independent of $x_{k,s}$.

$$\phi_{k,s} = \sum_{i=0, i \neq k}^{K-1} \sum_{l=0}^{L_{ic}-1} g_{j,l} x_{i,s-\tau_{i,l}} + \sum_{i=0, i \neq k}^{K-1} \sum_{l=0}^{L_{ddc}-1} g_{j,l} x_{i,s-\tau_{i,l}}. \quad (11)$$

By leveraging matched filtering [4] and IDFT, (10) can be simplified as **Theorem 2.1**. Specifically, the matched filter of length P is defined as $\mathcal{H}_{k,s} = c_{k,P-s}^*$, where $c_{k,s}^*$ is derived by applying the IDFT to the normalized measured data $C_{k,n}$. It can be easily proved that $c_{k,s}^*$ is also normalized i.i.d.

Theorem 2.1: After matched filtering and DFT, the Doppler and the delay can be decoupled and the received signal can be approximated as

$$A_{k,n} = \alpha B_{k,n} e^{j2\pi T_o f_d} e^{-j \frac{2\pi n(\tau_k + P)}{N}} e^{j\psi} + Z_{k,n}, \forall k \in \mathcal{K}, n \in \mathcal{N}, \quad (12)$$

where α denotes subcarrier attenuation coefficient and $Z_{k,n}$ denotes the AWGN with distribution $\mathcal{N}(0, \sigma_z^2)$.

Proof: Please refer to Appendix A. ■

Theorem 2.2: The CRLBs on the estimation MSEs of distance d_k and velocity v_k can be approximated by

$$\text{var}(\hat{d}_k) \geq \frac{3\sigma_z^2 c_o^2}{8\pi^2 \Delta f^2 \|\mathbf{B}_k\|^2 \alpha^2 MN (N^2 - 1)} = \text{CRLB}(\hat{d}_k), \quad (13)$$

$$\text{var}(\hat{v}_k) \geq \frac{3\sigma_z^2 c_o^2}{8\pi^2 T_o^2 f_c^2 \|\mathbf{B}_k\|^2 \alpha^2 MN (M^2 - 1)} = \text{CRLB}(\hat{v}_k). \quad (14)$$

Proof: Please refer to Appendix B. ■

Given the sensing MSE threshold η_k and ξ_k , the sensing quality requirement of the k -th device is $\text{CRLB}(\hat{d}_k) \leq \eta_k$ and $\text{CRLB}(\hat{v}_k) \leq \xi_k$. Let $\eta'_k = \frac{3\sigma_z^2 c_o^2}{8\eta_k \pi^2 \Delta f^2 \|\mathbf{B}_k\|^2 \alpha^2 MN (N^2 - 1)}$, $\xi'_k = \frac{3\sigma_z^2 c_o^2}{8\xi_k \pi^2 T_o^2 f_c^2 \|\mathbf{B}_k\|^2 \alpha^2 MN (M^2 - 1)}$, $\rho'_k = \min(\eta'_k, \xi'_k)$ and $\rho_k = \frac{1}{\rho'_k}$, the CRLB above constraint can be equivalently derived as $\|\mathbf{B}_k\|^{-2} \leq \rho_k, \forall k \in \mathcal{K}$.

B. Problem Formulation

Our goal is to jointly optimize the transmitting vector \mathbf{B}_k and the aggregation vector \mathbf{W} to minimize the MSE under the constraints of maximum power and CRLB. Mathematically, the following optimization problem is formulated

$$(P1) \quad \min_{\{\mathbf{B}_{k,n}, \mathbf{W}_n\}_{k \in \mathcal{K}}^{n \in \mathcal{N}}} \overline{\text{MSE}} \quad (15a)$$

$$\text{subject to} \quad \|\mathbf{B}_k\|^2 \leq P_t, \forall k \in \mathcal{K}, \quad (15b)$$

$$\|\mathbf{B}_k\|^{-2} \leq \rho_k, \forall k \in \mathcal{K}, \quad (15c)$$

The problem is non-convex due to the coupling between $\mathbf{B}_{k,n}$ and \mathbf{W}_n in the objective function. Moreover, the inequality constraint (15c) renders the feasible region non-convex. Therefore, it is challenging to obtain the globally optimal solution for (P1). Furthermore, both constraints cannot be simultaneously active. To ensure the solvability of the problem, we have $\rho_k \leq P_t$.

III. PROPOSED SOLUTION

In this section, we propose a two-phase iterative optimization algorithm to solve (P1). This algorithm consists of two phases: SCA-based AO phase and ADMM-based refinement phase.

A. SCA-Based Alternating Optimization Phase

Alternating optimization can be used to decompose (P1) into two more tractable subproblems. Initially, we align the phase as $\mathbf{B}_{k,n} = \mathcal{B}_{k,n} \times \frac{\mathbf{H}_{k,n}^H \mathbf{W}_n}{\|\mathbf{W}_n^H \mathbf{H}_{k,n}\|}$ to minimize the MSE [7]. The first subproblem focuses on optimizing \mathbf{W}_n given $\mathbf{B}_{k,n}$, which can further be partitioned into the following N subproblems

$$(P1.1) \quad \min_{\{\mathbf{W}_n\}} \sum_{k=0}^{K-1} |\mathbf{W}_n^H \mathbf{H}_{k,n} \mathbf{B}_{k,n} - 1|^2 + \|\mathbf{W}_n\|^2 \sigma_\Omega^2. \quad (16)$$

It is an unconstrained problem. The optimal \mathbf{W}_n^* can be obtained according to first-order condition as

$$\mathbf{W}_n^* = \left(\sum_{k=0}^{K-1} |\mathbf{B}_{k,n}|^2 |\mathbf{H}_{k,n}|^2 + \sigma_\Omega^2 \right)^{-1} \sum_{k=0}^{K-1} \mathbf{H}_{k,n} \mathbf{B}_{k,n}. \quad (17)$$

The second subproblem aims to optimize $\mathcal{B}_{k,n}$ given \mathbf{W}_n , which can be decomposed into the following K subproblems.

$$(P1.2) \quad \min_{\{\mathcal{B}_{k,n}\}} \sum_{n=0}^N (|\mathbf{W}_n^H \mathbf{H}_{k,n}| \mathcal{B}_{k,n} - 1)^2 + \|\mathbf{W}_n\|^2 \sigma_\Omega^2. \\ \text{subject to} \quad (15b)(15c) \quad (18)$$

When sensing constraints of (P1.2) are removed, this problem becomes a quadratically constrained quadratic programming (QCQP) problem, which is a convex problem. Let μ_k denote the dual variable associated with the transmit power constraint, we have the following theorem.

Theorem 3.1: When $P_t \rightarrow \infty$, we have $\mathbf{W}_n^* \rightarrow 0$ and thus the asymptotic $\overline{\text{MSE}} \rightarrow 0$ (lower bound).

Proof: Please refer to Appendix C. ■

When considering the sensing constraint, the problem becomes non-convex. The non-convexity stems from the non-convex feasible region. To tackle this issue, we use the SCA method based on the first-order Taylor expansion as

$$(\|\mathbf{B}_k^i\|^2 + 2\mathbf{B}_k^i (\mathbf{B}_k - 2\mathbf{B}_k^i))^{-1} \leq \rho_k, \forall k \in \mathcal{K}, \quad (21)$$

where \mathbf{B}_k^i represents a feasible reference point on the boundary of CRLB constraint. Moreover, $\|\mathbf{B}_k^i\|^2 + 2\mathbf{B}_k^i (\mathbf{B}_k - 2\mathbf{B}_k^i)$ acts as an upper bound for $\|\mathbf{B}_k\|^2$. Then, this subproblem becomes a QCQP, which can be solved by the existing toolbox, such as CVX.

Finally, (P1) is relaxed into two separate convex subproblem, whose feasible region is a subset of that of (P1).

Remark 1: Although SCA-based AO phase can obtain a suboptimal solution, it sacrifices part of the feasible region. As is shown in Fig. 2, the proportion of sacrifice increases, when P_t and ρ_k get closer. When $P_t \rightarrow \infty$ or $\text{CRLB} \rightarrow 0$ (e.g., $N \rightarrow \infty$), the feasible region sacrificed can be neglected.

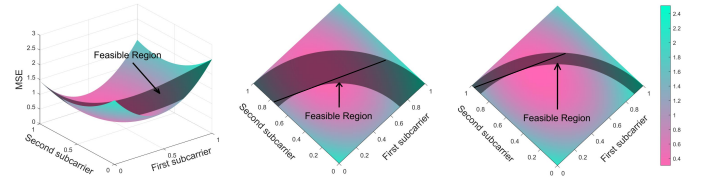


Fig. 2. Visualization of the feasible region in the SCA-based AO phase, taking a two-subcarrier system as an example.

B. ADMM-Based Refinement Phase

To search a broader feasible region and further improve the MSE, we adopt the ADMM method to refine $\mathcal{B}_{k,n}$ using the initial solution obtained from SCA-based AO phase. We use additional variables to transform inequality constraints into equality constraints [8, pp. 205-207]. Then, the augmented Lagrangian (AL) function can be obtained as (19), where λ_k and μ_k denote the Lagrangian dual variables associated with the constraints (15b) and (15c), respectively, and δ_k and β_k denote the penalty parameters. At the $(t+1)$ -th iteration, the ADMM algorithm consists of the primal updates, the dual updates and the penalty update steps. First is the primal updates, i.e.,

$$\mathcal{B}_{k,n}^{t+1} = \underset{\mathcal{B}_{k,n}^t}{\operatorname{argmin}} \mathcal{L}(\mathcal{B}_{k,n}^t, \lambda_k^t, \mu_k^t, \delta_k^t, \beta_k^t), \quad (22)$$

which can be solved by checking the first-order optimality conditions and its solution is given by (20). Then are the dual updates, i.e.,

$$\lambda_k^{t+1} = \max \left(0, \lambda_k^t + \delta_k^t \left(\|\mathcal{B}_k\|_2^2 - P_t \right) \right), \\ \mu_k^{t+1} = \max \left(0, \mu_k^t + \beta_k^t \left(\|\mathcal{B}_k\|_2^{-2} - \rho_k \right) \right), \quad (23)$$

Since the dual variables are non-negative, the max function is employed. In addition, it is impossible for both λ_k and μ_k to be zero simultaneously. This is because, as stated in Selection

$$\mathcal{L} = \sum_{n=1}^N (|\mathbf{W}_n^H \mathbf{H}_{k,n}| \mathcal{B}_{k,n} - 1)^2 + \frac{1}{2\delta_k} \left[\left(\max \left\{ 0, \lambda_k + \delta_k \left(\sum_{n=1}^N \mathcal{B}_{k,n}^2 - P_t \right) \right\} \right)^2 - \lambda_k^2 \right] + \frac{1}{2\beta_k} \left[\left(\max \left\{ 0, \mu_k + \beta_k \left(\left(\sum_{n=1}^N \mathcal{B}_{k,n}^2 \right)^{-1} - \rho_k \right) \right\} \right)^2 - \mu_k^2 \right] \quad (19)$$

$$\mathcal{B}_{k,n}^{t+1} = \left(|\mathbf{W}_n^H \mathbf{H}_{k,n}|^2 + \left[\lambda_k + \delta_k \left(\sum_{n=1}^N \mathcal{B}_{k,n}^2 - P_t \right) \right] 2\delta_k - 2\beta_k \left[\mu_k + \beta_k \left(\left(\sum_{n=1}^N \mathcal{B}_{k,n}^2 \right)^{-1} - \rho_k \right) \right] \left(\sum_{n=1}^N \mathcal{B}_{k,n}^2 \right)^{-2} \right)^{-1} \mathbf{W}_n^H \mathbf{H}_{k,n} \quad (20)$$

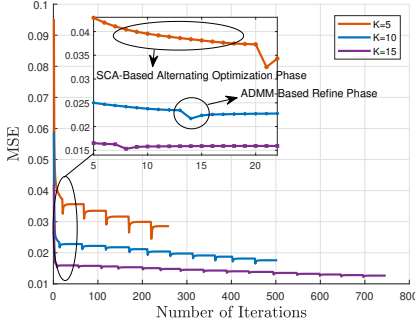
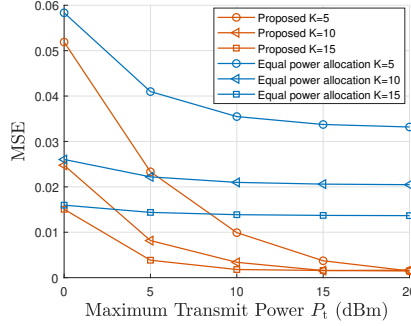
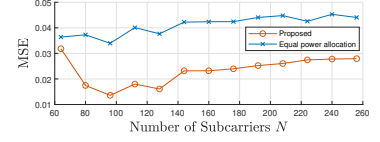
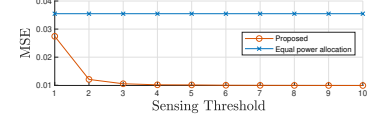
Fig. 3. Convergence behavior of **Algorithm 1**.Fig. 4. MSE versus the transmit power P_t .Fig. 5. MSE versus the number of subcarriers N .

Fig. 6. MSE versus the sensing thresholds.

II-B, the two constraints cannot be active simultaneously. Finally are the penalty updates, i.e.,

$$\delta_k^{t+1} = \begin{cases} \mathcal{G}\delta_k^t, & \Gamma_{pv} > \epsilon_{pc} \\ \mathcal{D}\delta_k^t, & \Gamma_{pv} \leq \epsilon_{pc}, \beta_k^{t+1} = \begin{cases} \mathcal{G}\beta_k^t, & \Gamma_{sv} > \epsilon_{sc} \\ \mathcal{D}\beta_k^t, & \Gamma_{sv} \leq \epsilon_{sc} \\ \beta_k^t, & \text{otherwise} \end{cases} \\ \delta_k^t, & \text{otherwise} \end{cases} \quad (24)$$

where \mathcal{G} and \mathcal{D} denote the growth and decay coefficients, Γ_{pv} and Γ_{sv} denote the violations of the power constraint and the sensing constraint, and ϵ_{pc} and ϵ_{sc} denote the maximum thresholds of the constraint violations.

Algorithm 1 Two-Phase Iterative Optimization Algorithm .

- 1: **Initialize** $\mathcal{B}_{k,n}^0, \mathbf{W}^0, \lambda^0, \mu^0, \delta^0, \beta^0, \epsilon_{mse}, \epsilon_{pc}, \epsilon_{sc}$.
 - 2: **Output** $\mathcal{B}_{k,n}^*$, \mathbf{W}^* .
 - 3: ****SCA-Based Alternating Optimization Phase****
 - 4: **repeat**
 - 5: Update \mathbf{W} using (17);
 - 6: Update \mathbf{B}_k via CVX with fixed \mathbf{W}
 - 7: **until** the reduction in MSE is less than ϵ_{MSE}
 - 8: ****ADMM-Based Refinement Phase****
 - 9: **for** $k = 1$ to K **do**
 - 10: **repeat**
 - 11: Update $\mathcal{B}_{k,n}^{t+1}$ using (20).
 - 12: Update $\lambda_k^{t+1}, \mu_k^{t+1}, \delta_k^{t+1}, \beta_k^{t+1}$ using (23).
 - 13: Update $\delta_{t+1}, \beta_{t+1}$ using (24).
 - 14: $t = t + 1$.
 - 15: **until** the reduction in MSE is less than ϵ_{MSE} and $\Gamma_{pv} > \epsilon_{pc}$ and $\Gamma_{sv} > \epsilon_{sc}$
 - 16: **end for**
-

The details of the proposed method are summarized in **Algorithm 1**. The complexity analysis of **Algorithm 1** is given as follows. The complexity for SCA-based AO phase is dominated by QCQP, whose worst-case complexity $\mathcal{O}(K^{4.5}N^{4.5}\log(1/\epsilon))$ with a prefixed solution accuracy is ϵ [9]. As for ADMM-based refinement phase, the calculation of $\mathcal{B}_{k,n}$ has a complexity of $\mathcal{O}(KN)$.

IV. NUMERICAL RESULTS

In this section, the numerical results are given to evaluate the performance of our proposed method. In the simulation, we set $P_t = 10$ dBm, $\sigma_{\Omega}^2 = -20$ dBm, $\eta_k = 1$, $\xi_k = 1$, $K = 5$, $M = 50$, $N = 64$, $T_o = 8 \mu s$, and $\Delta f = 156.25$ kHz.

For comparison, we consider *equal power allocation* $\mathbf{B}_{k,n} = \sqrt{\frac{P_t}{N}} \frac{\mathbf{H}_{k,n}^H \mathbf{W}_n}{\|\mathbf{W}_n^H \mathbf{H}_{k,n}\|}$ as the baseline, i.e., equal division of the maximum power for each subcarrier. Moreover, aggregation vectors \mathbf{W} are the same as the proposed method.

Fig. 3 shows the convergence behavior of the proposed **Algorithm 1**. We can observe that the convergence of the algorithm is divided into two phases. There are K distinct falling edges in stage ADMM-Based refinement phase, which correspond to device-by-device optimization given \mathbf{W}_n^* . Additionally, as K increases, the lower bound of the convergent MSE becomes smaller. It is equivalent to convergence for scenarios where federated learning (FL) is utilized for deep neural network (DNN) training [2].

Fig. 4 shows the MSE versus the transmit power P_t . It is observed that the proposed method outperforms the baseline. As the transmit power increases, the proposed method can approach the MSE lower bound more effectively. Furthermore, the MSE gap between the two methods increases as P_t increases. This is because the proposed method has a better signal magnitude alignment, which dominates MSE in the high transmit power regime.

Fig. 5 shows the MSE versus the number of subcarriers N . From this figure, we have three observations. Firstly, regardless of the value of N , the proposed method outperforms the baseline. Secondly, as N increases, the performance of the baseline deteriorates. This is because noise-induced error dominates MSE in the large number of N regime and it is difficult to design one common \mathbf{W} for all subcarriers. Finally, the MSE of the proposed method initially decreases and then increases along with the increase of N . The reason is that the number of subcarriers N has a dual impact on the MSE: (1). it affects the size of the feasible region, thereby influencing the quality of the initial solution in SCA-Based AO phase; (2). designing a common \mathbf{W} becomes more challenging as N increases. This verifies **Remark 1**.

Fig. 6 demonstrates the performance trade-off between computation and sensing. The results are obtained by setting different sensing thresholds. It is evident that the baseline remains unaffected by the sensing thresholds because it simply divides the maximum power equally. However, the MSE decreases as the sensing threshold rises in the proposed method.

V. CONCLUSION

In this letter, the problem of jointly designing transmitting vector and aggregation vector is addressed for the OFDM-based ISCC system. A two-phase iterative optimization algorithm is proposed to optimize transceiver vectors and minimize

the computational MSE under CRLB and power constraints. In the first phase, an SCA-based AO algorithm is adopted to decouple transceiver vectors and relax the feasible region. Based on the suboptimal solutions, we further improve MSE by refining transmitting vector under the full feasible region. Simulations and analysis have shown that the proposed algorithm is promising to achieve a better computing-sensing trade-off.

APPENDIX

A. Proof of Theorem 2.1

Assumption 1: The relative time gaps between any two multipaths are very small in comparison to the actual roundtrip delays, i.e., $\tau_{k,l} = \tau_{k,0}, \forall l$ [10]. Similarly, the attenuation coefficient gaps are also very small.

Firstly, matched filtering is employed under M observed OFDM symbols as

$$\begin{aligned} \mathbb{E}[u_{k,s}] &= \mathbb{E}\left[\left(\sum_{l=0}^{L_{\text{trc}}-1} g_{k,l} x_{k,s-\tau_{k,l}} e^{j2\pi T_o f_d} e^{j\psi} + \phi_{k,s} + \bar{z}_{k,s}\right) * \mathcal{H}_{k,s}\right] \\ &\stackrel{(a)}{\approx} \frac{1}{M} \sum_{m=0}^{M-1} \left(\sum_{l=0}^{L_{\text{trc}}-1} g_{k,l} x_{k,s-\tau_{k,0}} e^{j2\pi T_o f_d} e^{j\psi} + \phi_{k,s} + \bar{z}_{k,s}\right) * \mathcal{H}_{k,s} \\ &\stackrel{(b)}{\approx} \frac{1}{M} \sum_{m=0}^{M-1} \left[\sum_{p=0}^{P-1} \left(\sum_{l=0}^{L_{\text{trc}}-1} g_{k,l} x_{k,s-p-\tau_{k,0}} e^{j2\pi T_o f_d} e^{j\psi}\right) c_{k,P-p}^*\right] + z_{k,s} \\ &= u'_{k,s}, \end{aligned} \quad (25)$$

where $z_{k,s} = \frac{1}{M} \sum_{m=0}^{M-1} \sum_{p=0}^{P-1} \bar{z}_{k,j} c_{k,P-p}^*$ denotes the AWGN with distribution $\mathcal{N}(0, \sigma_z^2)$. (a) is founded on the law of large-number when M is large and **Assumption 1**. (b) follows that $c_{k,s}^*$ is normalized i.i.d.

Then, by applying the DFT to (25), we have

$$\begin{aligned} A_{k,n} &= \frac{1}{\sqrt{N}} \sum_{s=0}^{N-1} u'_{k,s} e^{-j\frac{2\pi n s}{N}} \\ &\stackrel{(a)}{\approx} G_{k,n} B_{k,n} e^{j2\pi T_o f_d} e^{-j\frac{2\pi n(\tau_{k,0}+P)}{N}} e^{j\psi} + Z_{k,n} \end{aligned} \quad (26)$$

where $Z_{k,n} = \frac{1}{\sqrt{N}} \sum_{s=0}^{N-1} \sum_{l=0}^{L_{\text{trc}}-1} z_{k,s} e^{-j\frac{2\pi n s}{N}}$ denotes the AWGN with distribution $\mathcal{N}(0, \sigma_z^2)$ and $G_{k,n} = \frac{1}{\sqrt{N}} \sum_{s=0}^{N-1} \sum_{l=0}^{L_{\text{trc}}-1} g_{k,l} e^{-j\frac{2\pi n s}{N}}$ denotes the subcarrier attenuation coefficient. Since **Assumption 1**, we have $G_{k,n} = G_{k,0}, \forall n \in \mathcal{N}$. The $G_{k,0}$ is equivalent to the constant coefficient $\alpha = \sqrt{\frac{c_0 \sigma_{\text{RCS}}}{(4\pi)^3 d_k^4 f_c^2}}$ [11], where σ_{RCS} denotes the radar cross section, d_k is the distance between the k -th device and the target, c_0 denotes the speed of light and f_c denotes the carrier frequency. Additionally, (a) follows $c_{k,s}^*$ is normalized i.i.d and the assumption that f_d is far less than subcarrier spacing Δf [12]. (26) shows that doppler shift and the delay are decoupled.

B. Proof of Theorem 2.2

For the convenience of analysis, we denote $\bar{\tau} = 2\pi\Delta f\tau_{k,0}$ and $\bar{v} = 2\pi T_o f_d$. Let $\theta = [\bar{\tau}, \bar{v}, \alpha, \psi]^T$ and $\mathcal{A}_{k,n}(\theta)$ denote the log likelihood function of $A_{k,n}$, the second-order Fisher information matrix is

$$\mathcal{J}_{ij} = \frac{1}{\sigma_z^2} \sum_{m=0}^{M-1} \sum_{n=0}^{N-1} \left[\frac{\partial \mathcal{A}_{k,n}^{\text{Re}}}{\partial \theta_i} \frac{\partial \mathcal{A}_{k,n}^{\text{Re}}}{\partial \theta_j} + \frac{\partial \mathcal{A}_{k,n}^{\text{Im}}}{\partial \theta_i} \frac{\partial \mathcal{A}_{k,n}^{\text{Im}}}{\partial \theta_j} \right], \quad (27)$$

where θ_i is the i -th entry of vector θ , upper subscript Re and Im denote the real and imaginary parts of $\mathcal{A}_{k,n}$.

Then, we can derive CRLB the inverse of the above Fisher information matrix as

$$\text{var}(\hat{\theta}_i) \geq \mathcal{J}^{-1}(i, i). \quad (28)$$

Given the complexity of the inverse processing, it is difficult to derive the closed-form CRLB from (28). Here, we use averaged CRLB provided by [11, chapter 3.3], which is based on the fact that each OFDM symbol can be used for one estimation and the average of all estimations is unbiased. Hence, we have

$$\text{var}(\hat{\theta}_i) \geq \frac{1}{MN} \mathcal{J}_{\theta_i}^{-1}(i, i), \quad (29)$$

where $\mathcal{J}_{\theta_1} = \frac{1}{\sigma_z^2} \sum_{n=0}^{N-1} \left[\frac{\partial \mathcal{A}_{k,n}^{\text{Re}}}{\partial \theta_i} \frac{\partial \mathcal{A}_{k,n}^{\text{Re}}}{\partial \theta_j} + \frac{\partial \mathcal{A}_{k,n}^{\text{Im}}}{\partial \theta_i} \frac{\partial \mathcal{A}_{k,n}^{\text{Im}}}{\partial \theta_j} \right], i, j \in \{1, 3, 4\}$ and $\mathcal{J}_{\theta_2} = \frac{1}{\sigma_z^2} \sum_{n=0}^{M-1} \left[\frac{\partial \mathcal{A}_{k,n}^{\text{Re}}}{\partial \theta_i} \frac{\partial \mathcal{A}_{k,n}^{\text{Re}}}{\partial \theta_j} + \frac{\partial \mathcal{A}_{k,n}^{\text{Im}}}{\partial \theta_i} \frac{\partial \mathcal{A}_{k,n}^{\text{Im}}}{\partial \theta_j} \right], i, j \in \{2, 3, 4\}$. By substituting (12) into (29), we have

$$\text{var}(\hat{\tau}) \geq \frac{6\sigma_z^2}{\|\mathbf{B}_k\|^2 \alpha^2 MN (N^2 - 1)}, \quad (30)$$

$$\text{var}(\hat{v}) \geq \frac{6\sigma_z^2}{\|\mathbf{B}_k\|^2 \alpha^2 MN (M^2 - 1)}. \quad (31)$$

Since $d_k = \frac{1}{2} c_0 \tau_{k,0}$ and $\tau_{k,0} = \frac{1}{2\pi\Delta f} \bar{\tau}$, we have $d_k = \frac{c_0}{4\pi\Delta f} \bar{\tau}$ and further derive (13). Since $f_d = \frac{2v_k f_c}{c_0}$ and $\bar{v} = 4\pi T_o \frac{v f_c}{c_0}$, we have (14).

C. Proof of Theorem 3.1

The Lagrangian of the second subproblem is

$$\mathcal{L}_1(\mathbf{B}_{k,n}, \mu_k) = \sum_{n=1}^N (|\mathbf{W}_n^H \mathbf{H}_{k,n}| \mathbf{B}_{k,n} - 1)^2 + \mu_k \left(\sum_{n=1}^N \mathbf{B}_{k,n}^2 - P_t \right). \quad (32)$$

By leveraging the stationarity of Karush-Kuhn-Tucker (KKT) conditions, the optimal solution is $\mathbf{B}_{k,n}^* = \frac{|\mathbf{W}_n^H \mathbf{H}_{k,n}|}{|\mathbf{W}_n^H \mathbf{H}_{k,n}|^2 + \mu_k^*}$, where μ_k^* is the optimal dual variable. By leveraging the complementary slackness condition $\mu_k^* \left(\sum_{n=1}^N \mathbf{B}_{k,n}^2 - P_t \right) = 0$, we have $\mu_k^* \rightarrow 0$ and $\mathbf{W}_n^* \rightarrow 0$ when $P_t \rightarrow \infty$. By substituting them into (15a), we have the asymptotic $\overline{\text{MSE}} \rightarrow 0$.

REFERENCES

- [1] F. Liu, Y. Cui, C. Masouros, J. Xu, T. X. Han, Y. C. Eldar, and S. Buzzi, "Integrated sensing and communications: Towards dual-functional wireless networks for 6G and beyond," *IEEE J. Sel. Areas Commun.*, vol. 40, no. 6, pp. 1728–1767, 2022.
- [2] D. Wen, Y. Zhou, X. Li, Y. Shi, K. Huang, and K. B. Letaief, "A survey on integrated sensing, communication, and computation," *IEEE Comm. Surv. Tutor.*, 2024.
- [3] Q. Qi, X. Chen, C. Zhong, and Z. Zhang, "Integrated sensing, computation and communication in B5G cellular internet of things," *IEEE Trans. Wireless Commun.*, vol. 20, no. 1, pp. 332–344, 2020.
- [4] X. Li, F. Liu, Z. Zhou, G. Zhu, S. Wang, K. Huang, and Y. Gong, "Integrated sensing, communication, and computation over-the-air: MIMO beamforming design," *IEEE Trans. Wireless Commun.*, vol. 22, no. 8, pp. 5383–5398, 2023.
- [5] K. Dong, S. A. Vorobyov, H. Yu, and T. Taleb, "Beamforming design for integrated sensing, over-the-air computation, and communication in internet of robotic things," *IEEE Internet Things J.*, vol. 11, no. 20, pp. 32478–32489, 2024.
- [6] Z. Zhuang, D. Wen, Y. Shi, G. Zhu, S. Wu, and D. Niyato, "Integrated sensing-communication-computation for over-the-air edge AI inference," *IEEE Trans. Wireless Commun.*, vol. 23, no. 4, pp. 3205–3220, 2023.
- [7] Y. Chen, H. Xing, J. Xu, L. Xu, and S. Cui, "Over-the-air computation in OFDM systems with imperfect channel state information," *IEEE Trans. Commun.*, vol. 72, no. 5, pp. 2929–2944, 2023.
- [8] A. J. Conejo, E. Castillo, R. Minguez, and R. Garcia-Bertrand, *Decomposition techniques in mathematical programming: engineering and science applications*. Springer Science & Business Media, 2006.

- [9] Y. Huang and D. P. Palomar, "Randomized algorithms for optimal solutions of double-sided QCQP with applications in signal processing," *IEEE Trans. Signal Process.*, vol. 62, no. 5, pp. 1093–1108, 2014.
- [10] S. Sen and A. Nehorai, "Adaptive OFDM radar for target detection in multipath scenarios," *IEEE Trans. Signal Process.*, vol. 59, no. 1, pp. 78–90, 2010.
- [11] K. M. Braun, "OFDM radar algorithms in mobile communication networks," Ph.D. dissertation, Karlsruhe, Karlsruher Institut für Technologie (KIT), Karlsruhe, Germany, 2014.
- [12] L. Gaudio, M. Kobayashi, B. Bissinger, and G. Caire, "Performance analysis of joint radar and communication using OFDM and OTFS," in *Proc. IEEE Int. Conf. Commun. Workshops (ICC Workshops)*, 2019, pp. 1–6.